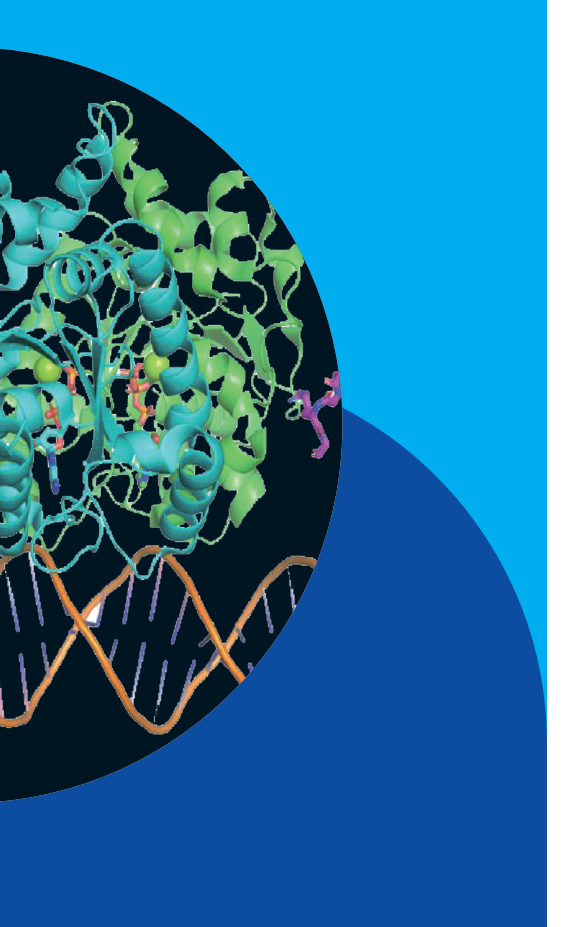
### Life Science



Despite advancements in computational techniques, which were recognized by the 2024 Nobel Prize in Chemistry for groundbreaking work, and cryo-EM methods, synchrotron macromolecular crystallography remains an indispensable tool for revealing the intricate atomic structures of biomolecules. This high-resolution structural information is crucial for understanding the structure–function relationships, as well as for driving various scientific applications, from elucidating complex biological mechanisms to supporting drug development and analyzing bio-samples to unravel unsolved issues in biology.

The NSRRC in Taiwan maintains a robust infrastructure to support this field, featuring three specialized protein beamlines—TLS 15A1, TPS 05A, and TPS 07A—that are accessible to a broad community of users. Starting in 2025, the TPS 05A and TPS 07A beamlines will undergo an upgrade program, which will enable them to provide more diverse functionalities to meet the evolving needs of users better. Furthermore, the NSRRC offers a diverse array of specialized beamlines, including those for small-angle X-ray scattering (TPS 13A), soft X-ray tomography (TPS 24A), transmission X-ray microscopy (TPS 31A), quick-scanning X-ray absorption spectroscopy (TPS 44A), white X-ray (TLS 01A1), X-ray microscopy (TLS 01B1), and infrared microspectroscopy (TLS 14A1), enabling researchers to tackle a broad range of biological problems.

The NSRRC user community enjoyed a banner year in 2024, delivering an array of significant scientific breakthroughs. Consequently, we have selected four exemplary studies conducted at our facilities to feature in this activity report. The first study, conducted by Yuh-Ju Sun and Chwan-Deng Hsiao, examined the distinct molecular systems—ParABS in bacteria and Seg filaments in archaeaused by single-celled organisms to ensure accurate DNA partitioning during cell division, revealing the complex and elegant survival solutions even in the simplest life forms. The second study, conducted by Ming-Hon Hou, investigated using bidirectional bis-intercalating acridine compounds to target DNA junction sites as a potential anticancer strategy because these compounds can cross-link and stabilize DNA junctions, thereby disrupting cellular processes and inhibiting cancer cell proliferation. The third study was by Hui-Chun Cheng, who showed that H<sub>2</sub>S modification of PKM2 through cysteine 326 sulfhydration reduces its activity, impairs cancer cell division, and leads to tumor suppression, suggesting blocking this H<sub>2</sub>S-mediated PKM2 modification as a promising therapeutic approach for targeting cancer cell metabolism. Finally, the fourth study was by Shiou-Ru Tzeng, who revealed how the adaptor protein NlpI regulates the cell wall endopeptidase MepS to maintain bacterial cell wall integrity by modulating MepS activity and targeting it for degradation. (by Chun-Hsiang Huang)

# Two Ancient Solutions to One Modern Problem: DNA Management in Single-Celled Organisms

Single-celled bacteria and archaea use different but equally clever molecular systems to partition their DNA during cell division; bacteria with their ParABS motor system and archaea with their Seg filament system. These microscopic mechanisms show that even the simplest life forms have complex and elegant survival solutions.

ne of the most fundamental challenges in microscopic cellular life is ensuring accurate DNA partitioning during cell division. This process, much like dividing a vast library's contents between two new locations, requires intricate coordination and precise organization. To address this important scientific phenomenon, Yuh-Ju Sun (National Tsing Hua University) and Chwan-Deng Hsiao (Academia Sinica) collaborated by using various bioassays and protein crystallography techniques to reveal fascinating details regarding how single-celled organisms (bacteria and archaea) accomplish this crucial task. All crystallographic data were collected at **TLS 15A**, **TPS 05A**, and **TPS 07A** of the NSRRC.

Researchers have uncovered the sophisticated ParABS (*par* stands for partitioning) system in bacteria, consisting of three key components working in harmony. ParA acts as a molecular motor powered by ATP, ParB serves as a versatile DNA-binding protein, and the *parS* sequences function as specific DNA anchoring points.<sup>1</sup> In this study, the *Helicobacter pylori* ParB (*Hp*ParB) protein demonstrates remarkable adaptability, behaving like a skilled librarian who can both locate specific books and organize entire shelves. This versatility is controlled by CTP, which acts as a molecular switch. When CTP is absent, *Hp*ParB focuses on specific DNA sequences (*e.g.*, *parS*), but in its presence, *Hp*ParB can slide freely along DNA (**Fig. 1(a)**).

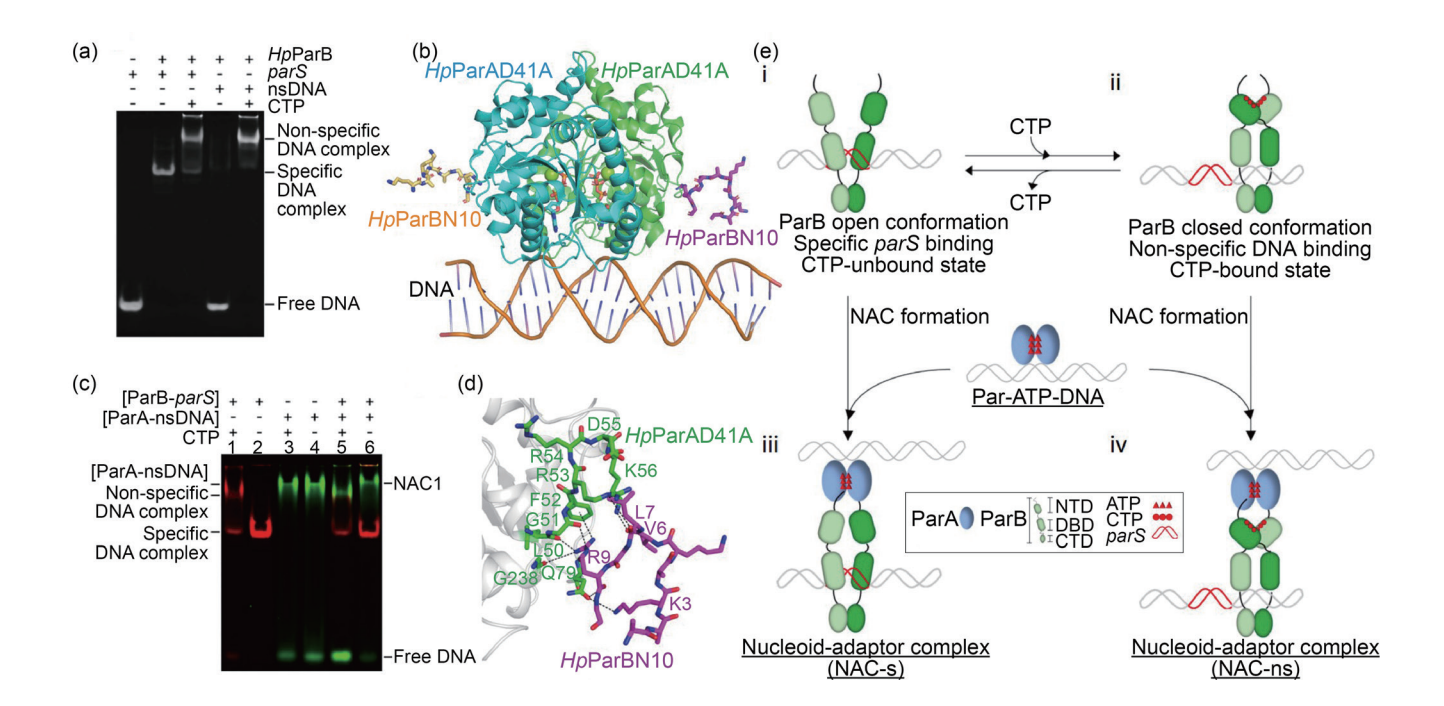


Fig. 1: (a) The electrophoretic mobility shift assay (EMSA) reveals *Hp*ParB's pattern for binding to *parS* and non-specific DNA, both with and without CTP present. (b) The *Hp*ParAD41A–DNA–*Hp*ParBN10 complex structure shows a cyan and green dimer, with orange and magenta *Hp*ParBN10 peptides bound to each monomer, alongside a wheat-colored DNA molecule. (c) EMSA analysis was performed to examine binding interactions between *Hp*ParB–*parS* and *Hp*ParA–nsDNA complexes. Initially, *Hp*ParB and *Hp*ParA were separately incubated with Cy3-labeled *parS* and Cy5-labeled nsDNA, respectively, either with or without CTP. These preformed complexes were then combined and further incubated under CTP-present or CTP-absent conditions before EMSA detection. (d) In the *Hp*ParAD41A–DNA–*Hp*ParBN10 complex, the magenta *Hp*ParBN10 binding site interacts with the grey *Hp*ParAD41A ribbon structure, where green-colored residues form key contacts marked by dashed lines. (e) The ParABS system model shows how green-colored ParB, containing three domains—the N-terminal domain (NTD), the DNA-binding domain (DBD), and the C-terminal domain (CTD)—adopts CTP-regulated open and closed conformations for specific (i) and non-specific (ii) DNA binding. When these Par–DNA complexes interact with purple-blue ParA–ATP–DNA, they form either specific NAC-s (iii) or non-specific NAC-ns (iv) nucleoid–adaptor complexes. [Reproduced from Ref. 1]

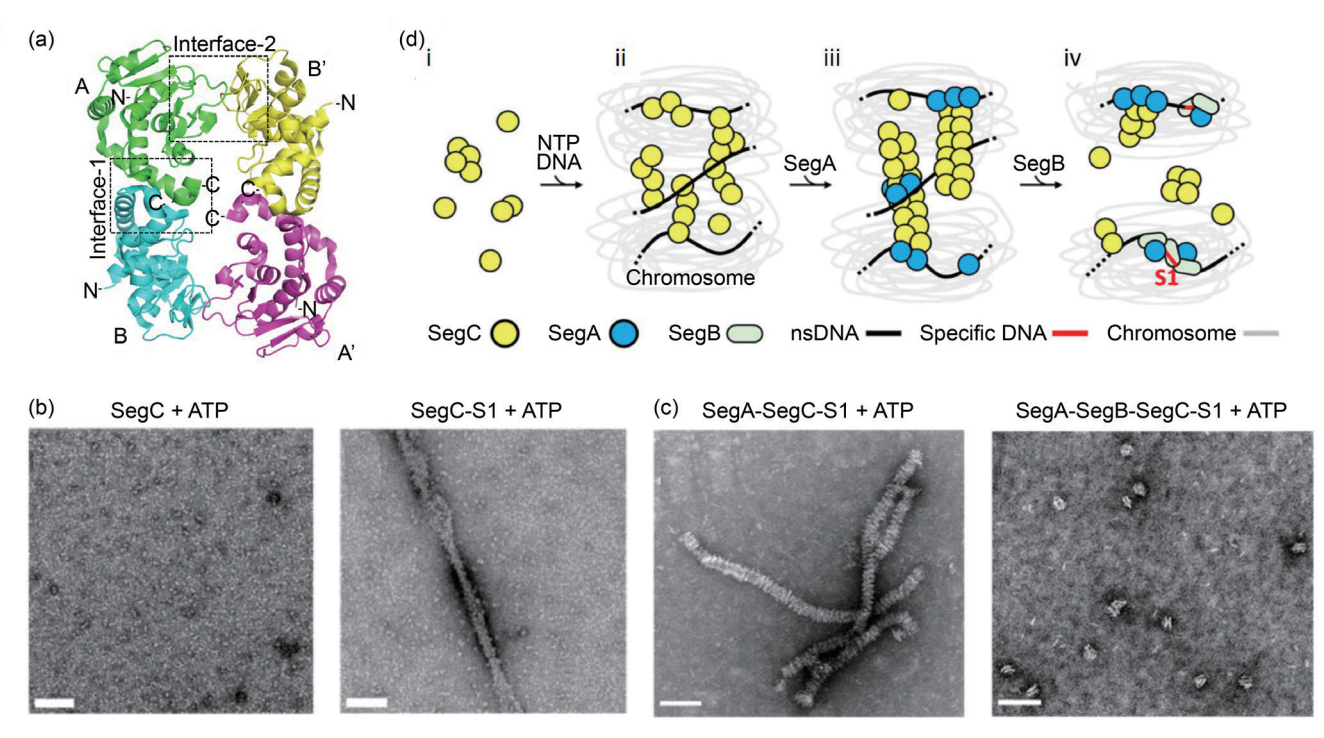


Fig. 2: (a) The SegC tetramer comprises four molecules (A, B, A', B') displayed in green, cyan, magenta, and yellow, respectively, with dimer interfaces marked by dotted squares as Interface-1 and Interface-2. (b) Negative-stain electron microscopy (EM) showing SegC structures with and without DNA and NTP. S1 (site 1) refers to a specific DNA sequence. (c) Negative-stain EM visualization of SegC, SegA, SegB, and DNA interactions. (d) A four-step model for SegC filament function: (i) Random distribution and multimerization of SegC in archaeal cells, (ii) NTP and DNA-dependent filament formation, (iii) SegA-mediated remodeling into higher-order filaments, and (iv) SegB-stimulated SegA ATPase activity leading to filament disassembly. [Reproduced from Ref. 2]

To improve our understanding of this system, researchers employed a clever strategy using a mutant form of *Hp*ParA (*Hp*ParAD41A) that displays a slower turnover rate, similar to using slow-motion photography to capture rapid movements. This approach revealed crucial details about how *Hp*ParA interacts with DNA and uses ATP for energy. *Hp*ParAD41A allowed scientists to observe the step-bystep process of how *Hp*ParA recognizes and binds to DNA, providing unprecedented insights into this fundamental mechanism (**Fig. 1(b)**).

One of the most significant discoveries in the bacterial system involves the formation of the nucleoid–adaptor complex (NAC; this term represents the composition of HpParA-HpParB-DNA). The research revealed that HpParA proteins form dimers when bound to CTP, creating a complex with DNA that can interact with HpParB through a specialized cation– $\pi$  interaction. This interaction, particularly between HpParB's Arg9 and HpParA's Phe52, proves essential for the entire system's functionality (**Figs. 1(b)** –**1(d)**).

The bacterial study also unveiled a detailed molecular mechanism where CTP acts as a master regulator. When CTP is absent, ParB maintains an "open" configuration, specifically binding to *parS* sequences and preparing to interact with the ParA–ATP–DNA complex. The introduction of CTP triggers ParB to adopt a "closed" form,

enabling it to slide along DNA non-specifically and interact more efficiently with ParA. This CTP-dependent switching mechanism is crucial for promoting ATP hydrolysis by ParA and ensuring proper system function (**Fig. 1(e)**).

Meanwhile, in the ancient world of archaea, researchers have discovered a different but equally fascinating system involving three proteins: SegA, SegB, and the newly identified SegC. Detailed structural analysis revealed that SegC has a unique architectural design that allows it to form both dimers (pairs) and tetramers (groups of four). This molecular architecture, particularly the protein's C-terminal region, proves crucial for its functionality—when researchers removed this tail end, SegC lost its ability to bind DNA and form filaments (Fig. 2(a)). The SegC protein shows the remarkable abilities, binding to DNA without sequence specificity and forming thread-like structures (filaments) when it encounters DNA and energy molecules (Fig. 2(b)).

The coordination between these components involves SegC working with SegA to form larger filaments in the presence of ATP, while SegB can break these structures apart when needed (Fig. 2(c)). The archaeal system's unique feature lies in SegC's ability to break down various energy molecules (NTPs), though the exact role of this capability remains under investigation. The researchers proposed a step-wise process where SegC forms initial filaments, SegA helps

organize these structures, and SegB eventually breaks them down to complete the DNA organization process (Fig. 2(d)).

The implications of this research extend far beyond basic science. Understanding these fundamental processes could lead to new strategies for controlling bacterial growth, potentially contributing to antibiotic developments. Furthermore, since archaea are considered ancient relatives of complex organisms, these findings provide valuable insights into how DNA organization evolved over time. (Reported by Chun-Hsiang Huang)

This report features the work of Yuh-Ju Sun and Chwan-Deng Hsiao published in Nucleic Acids Res. **52**, 7321 (2024) and Nucleic Acids Res. **52**, 9966 (2024).

TPS 05A Protein Microcrystallography
TPS 07A Micro-focus Protein Crystallography
TLS 15A1 Biopharmaceuticals Protein Crystallography

- Protein Crystallography
- Biological Macromolecules, Protein Structures, Life Science

#### References

- C.-H. Chu, C.-T. Wu, M.-G. Lin, C.-Y. Yen, Y.-Z. Wu, C.-D. Hsiao, Y.-J. Sun, Nucleic Acids Res. 52, 7321 (2024).
- M.-G. Lin, C.-Y. Yen, Y.-Y. Shen, Y.-S. Huang, I. W. Ng,
   D. Barillà, Y.-J. Sun, C.-D. Hsiao, Nucleic Acids Res. 52,
   9966 (2024).

### **Targeting DNA Junctions for Anticancer Drug Development**

DNA helix-helix junctions form tetraplex base pairs at the junction interface, serving as "hotspots" for bidirectional bis-intercalating agents. This study investigates the structural basis for targeting DNA junctions with acridine bis-intercalators as a potential anticancer strategy.

Biological processes such as recombination or replication can generate DNA juxtaposed helix–helix structures and duplex crossovers. These structures require topoisomerases to decatenate the interlinked DNA crossover sites. Within the crossover structures, the base pairs of the duplexes can interact with each other, resulting in novel junctions. Targeting DNA junction sites with bis-intercalating compounds containing bidirectional linkers could inhibit topoisomerase activity, therefore representing an effective anticancer strategy. Bidirectional bis-intercalators have the unique ability to insert their chromophores simultaneously into the base pairs of two DNA duplexes. This non-covalent bridging ability of small molecules enables them to cross-link DNA junctions, thereby disrupting biological processes critical for cellular function. However,

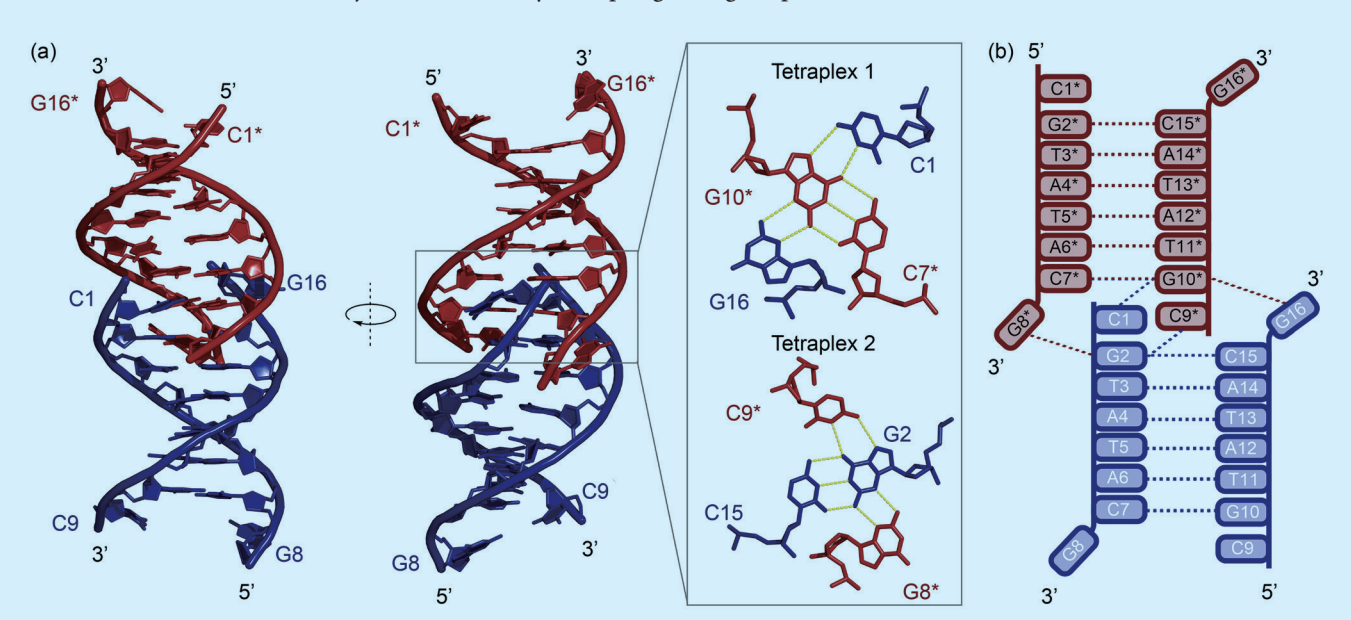


Fig. 1: Structural features of a d(CGTATACG)<sub>2</sub> DNA forming junction. (a) Crystal structure assembly of continuous duplexes forming an end-to-end helix-helix junction structure. One DNA duplex is shown in dark blue and the adjacent symmetry-related duplex is in dark red. Asterisks (\*) represent residues in the adjacent duplex. Two layered tetraplex base pairings at the junction interface are shown in an enlarged view. (b) Schematic representation of the crystal structure of d(CGTATACG)<sub>2</sub>, indicating the residues involved in junction formation. [Reproduced from Ref. 6]

the limited structural understanding of DNA junction formation and its interactions with small molecules has hindered the development of these targeted therapies.

The study by Ming-Hon Hou (National Chung Hsing University) and his team sheds light on the structural basis of DNA junction formation and provides valuable insights into targeting DNA junctions with bidirectional bis-intercalators for anticancer drug development.<sup>6</sup> The elucidation of the complex crystal structure required the access to a high-resolution X-ray facility housed at the NSRRC beamline **TLS 15A1**. Hou's team solved the crystal structure of d(CGTATACG)<sub>2</sub> DNA, which exhibited a unique duplex–duplex junction (**Fig. 1**). In the central region, the structure showed B-DNA-like right-handed features. Interestingly, the terminal CG base pairs contributed to forming a helix–helix junction with two tetraplex base pairs at the junction interface. Detailed analysis revealed that this structure closely resembles the duplex–duplex contacts in catenated DNA and that the tetraplex interface at the junction site serves as a "hotspot" capable of accommodating external ligands between the two neighboring duplexes.

Next, the team explored the possibility of targeting this junction structure with small-molecule compounds. Yih-Chern Horng (National Changhua University of Education) synthesized two alkyl-linked diaminoacridine compounds, DA4 and DA5 (**Fig. 2(a)**). Both DA4 and DA5 contain acridine chromophores connected by semi-flexible linkers that are four-and five-carbon long, respectively. These two acridine derivatives possess inter-duplex DNA intercalating properties. To investigate the binding mechanism of DA4 and DA5 with DNA, they determined the crystal structures of DA4 and DA5 with the d(CGTATACG)<sub>2</sub> sequence in the C222<sub>1</sub> and P2<sub>1</sub> space groups, respectively, at a resolution of 1.58 Å. As expected, in

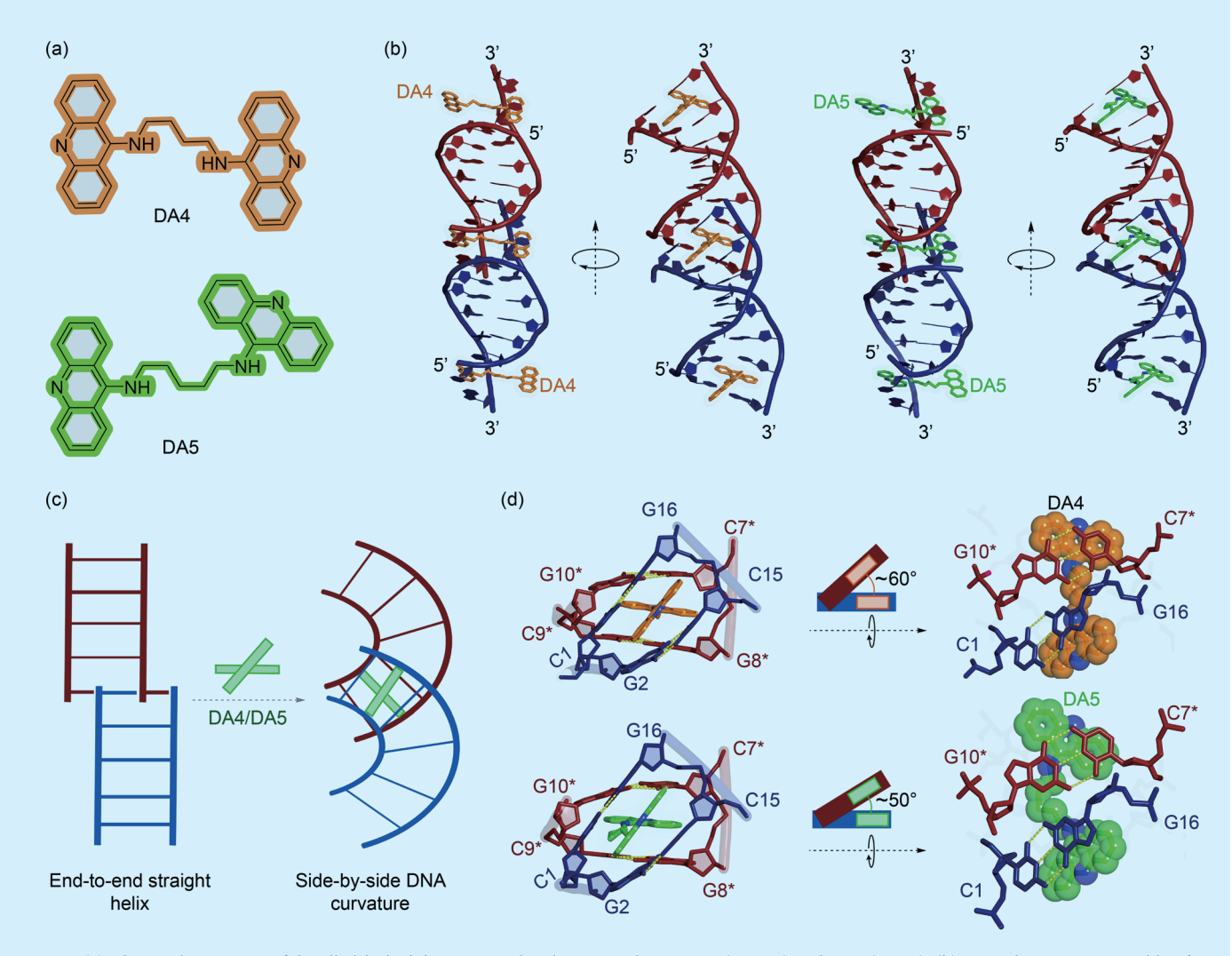


Fig. 2: (a) Chemical structures of the alkyl-linked diaminoacridine bis-intercalators DA4 (orange) and DA5 (green). (b) Crystal structure assembly of DA4–DNA and DA5–DNA complexes showing inter-duplex cross-linking of the DNA duplexes. (c) Schematic diagram showing topological changes in DNA upon intercalation of DA4 or DA5 at the terminal junction site. (d) Magnified view of the intercalation site shows the angled intercalation of DA4 and DA5 at the junction interface in steps C1pG2/C15pG16 in one duplex and C7\*pG8\*/C9\*pG10\* in the other adjacent duplex, viewed from the front and top. In DA4, the linker connecting the two acridine moieties is straight, whereas the linker in DA5 has a bent conformation. A single-atom difference in the linker of DA4 and DA5 led to distinct propeller geometries with approximately 60° and 50° between two ligands, respectively. [Reproduced from Ref. 6]

both crystal structures, the intercalation of DA4 or DA5 mediated DNA-DNA contacts and cross-linked adjacent duplexes (Fig. 2(b)). Compared to the unliganded native DNA junction structure, DA4 and DA5 induced significant changes in DNA topology, transforming it from an end-to-end straight helix to a side-by-side curved geometry (Fig. 2(c)). The cross-linking of DNA duplexes also caused a transition from the B-form to an A-form-like conformation, accompanied by bending and overwinding of the backbone. The different linker lengths and flexibilities of DA4 and DA5 resulted in distinct local structural and stabilizing effects on DNA. In the DA4-DNA complex, the four-carbon linker of DA4 adopted a straight geometry, while the DA5 linker bent toward one of the DNA backbones (Fig. 2(d)). This difference in linker flexibility caused the chromophores of DA4 and DA5 to stagger at different angles. In the DA4-DNA complex, the chromophores formed an angle of approximately 60° with the horizontal plane of the acridine ring, while in the DA5-DNA complex, the angle between the two acridine chromophores was approximately 50°. This flexibility of the DA5 linker allowed its chromophores to align more optimally, enabling continuous stacking interactions with DNA base pairs. Consequently, DA5 exhibited more stacking interactions with DNA than DA4. The bent linker and less tilted chromophore of DA5 brought its amino groups closer to the cytosine bases, facilitating a direct water-mediated interaction that likely resulted in a more stable complex with stronger binding. By contrast, the greater distance between the amino group of the DA4 linker and the keto group of cytosine in the DA4-DNA complex led to indirect and weaker water-mediated interactions. These findings suggest that DA5 induces stronger structural changes in DNA than DA4, potentially leading to stronger stabilizing effects. These results were further corroborated through biophysical experiments.

When tested in *in vitro* and *in vivo* models, the two acridine derivatives inhibited topoisomerase II activity, induced G2/M phase accumulation in the cell cycle, triggered apoptosis, and reduced cancer tumor growth, highlighting the anticancer potential of this mode of DNA binding. Notably, the results showed that DA5 exhibited more pronounced anticancer effects than DA4, likely due to its enhanced stability and stronger DNA-binding interactions at the junction. Through investigation of the structural basis for these results, Hou and his team demonstrated how small molecules can precisely target and stabilize DNA junction sites, inhibit topoisomerase activity, and impair cancer cell proliferation. These findings could guide the development of more effective derivatives in future, paving the way for targeting DNA–DNA duplex contacts through bis-intercalation. (Reported by Roshan Satange, National Chung Hsing University)

This report features the work of Ming-Hon Hou and his collaborators published in Nucleic Acids Res. 52, 9303 (2024).

#### TLS 15A1 Biopharmaceuticals Protein Crystallography

- X-ray Crystallography
- Biological Macromolecules, Cancer, DNA Junctions, Life Science

#### References

- 1. M. L. Martínez-Robles, G. Witz, P. Hernández, J. B. Schvartzman, A. Stasiak, D. B. Krimer, Nucleic Acids Res. 37, 5126 (2009).
- 2. G. Witz, A. Stasiak, Nucleic Acids Res. 38, 2119 (2009).
- 3. Y. Pommier, A. Nussenzweig, S. Takeda, C. Austin, Nat. Rev. Mol. Cell Biol. 23, 407 (2022).
- 4. E. Ivens, M. M. D. Cominetti, M. Searcey, Bioorg. Med. Chem. 69, 116897 (2022).
- 5. K. T. McQuaid, A. Pipier, C. J. Cardin, D. Monchaud, Nucleic Acids Res. 50, 12636 (2022).
- 6. S.-C. Huang, C.-W. Chen, R. Satange, C.-C. Hsieh, C.-C. Chang, S.-C. Wang, C.-L. Peng, T.-L. Chen, M.-H. Chiang, Y.-C. Horng, M.-H. Hou, Nucleic Acids Res. **52**, 9303 (2024).

## Breaking Cancer's Energy Code: New Insights into Hydrogen Sulfide and Pyruvate Kinase M2 Regulation

Hydrogen sulfide modifies the pyruvate kinase M2 enzyme at cysteine 326, affecting cancer cell metabolism. Blocking this modification reduces PKM2 activity and impairs cancer cell division, leading to complete tumor suppression.

Cancer cells undergo significant metabolic reprogramming that is primarily characterized by the Warburg effect. In this process, they prefer aerobic glycolysis over oxidative phosphorylation. Although this process is less efficient for ATP production, it provides essential metabolic intermediates for rapid cancer cell proliferation under nutrient-limited conditions.

The glycolytic pathway is regulated by three key enzymes, with the pyruvate kinase M2 (PKM2) playing a crucial role. PKM2, which is predominantly expressed in cancer cells, differs from PKM1's catalytic properties. While PKM1 maintains high activity as a tetramer, PKM2's activity is typically low in cancer cells because of various post-

translational modifications, which allow redirection of glucose metabolism toward biomass synthesis.

Recent research has focused on hydrogen sulfide (H<sub>2</sub>S), an endogenous gasotransmitter that shows concentration-dependent effects on cancer progression. H<sub>2</sub>S primarily functions through protein sulfhydration, a post-translational modification where H<sub>2</sub>S forms a persulfide (-SSH) bond on cysteine residues of target proteins.<sup>1</sup> At lower concentrations, H<sub>2</sub>S promotes tumor growth through multiple mechanisms, including antiapoptotic effects, DNA repair, and angiogenesis. However, higher concentrations can inhibit cancer cell proliferation.

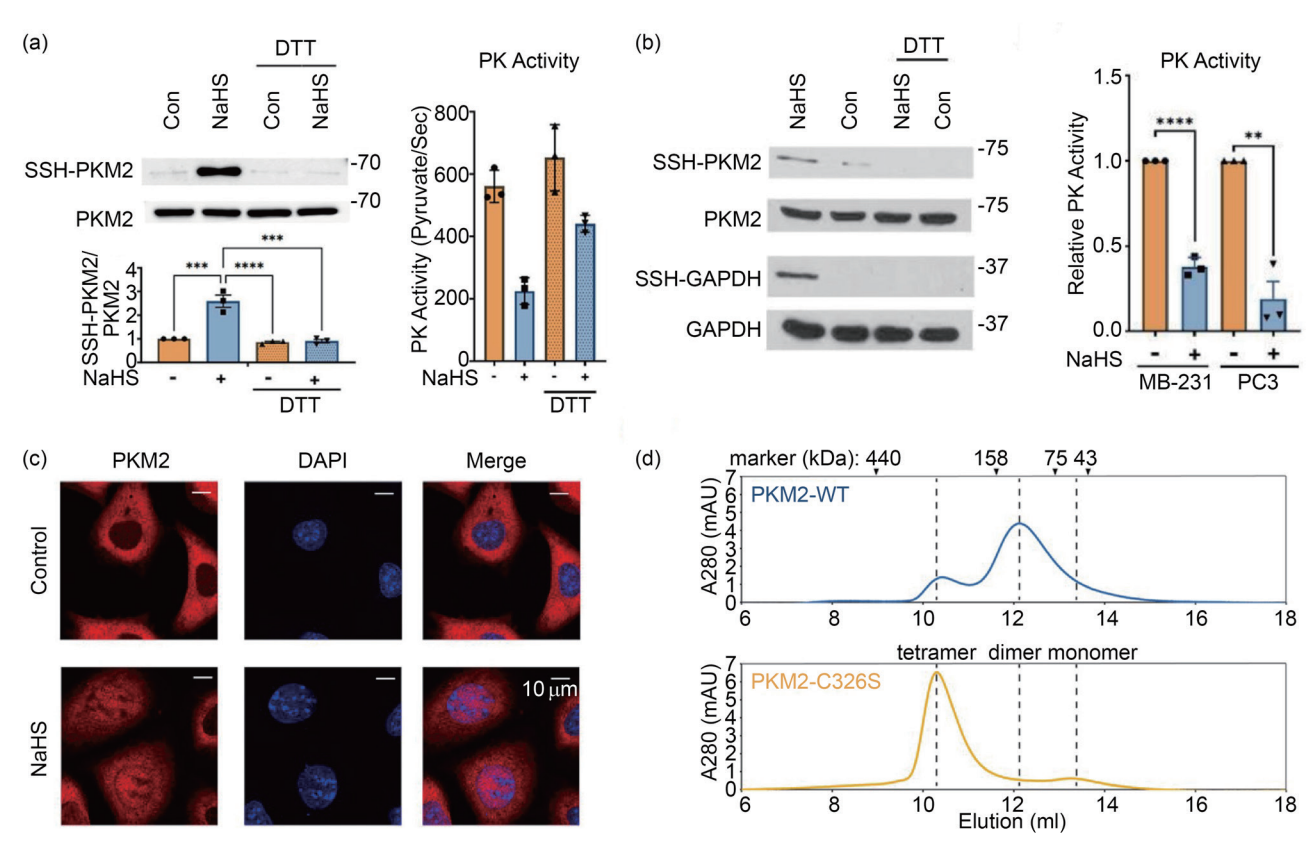


Fig. 1: (a) Results of two main analyses performed in the experimental study. The first part examined PKM2 sulfhydration in MDA-MB-231 cell lysates treated with NaHS and DTT by using a biotin switch assay followed by immunoblotting with an anti-PKM2 antibody. The second part investigated pyruvate kinase activity by measuring pyruvate production in recombinant PKM2 after treatment with NaHS and DTT under ice-cold conditions. (b) Results of the experiment investigating protein sulfhydration and enzymatic activity in two parts. The first part examined PC3 cell lysates treated with NaHS and DTT by using biotin switch assay and immunoblotting to detect sulfhydration of both PKM2 and GAPDH (used as a positive control). The second part focused on measuring pyruvate kinase activity in both MDA-MB-231 and PC3 cell lysates after NaHS treatment, specifically by quantifying pyruvate production. (c) Treatment of MDA-MB-231 cells with NaHS and visualization of PKM2 localization using immunocytochemistry with DAPI nuclear staining (scale: 10 µm). (d) Results of gel filtration analysis of PKM2 proteins (WT and C326S mutant) performed without FBP to examine their oligomeric states. [Reproduced from Ref. 2]

The interplay between H<sub>2</sub>S and PKM2 represents a fascinating area of research, particularly given that PKM2 activity can be inhibited by L-cysteine, which serves as the primary source for H<sub>2</sub>S production. This intricate connection, which is mediated through protein sulfhydration, reveals a critical regulatory mechanism in cancer cell metabolism. The emerging understanding of how H<sub>2</sub>S-mediated protein sulfhydration influences cancer progression has opened promising new avenues for therapeutic interventions that specifically target cancer-specific metabolic pathways. To further explore this novel regulatory mechanism, Lu-Hai Wang (China Medical University), Hui-Chun Cheng (National Tsing Hua University), and Kai-Ti Lin (National Tsing Hua University) launched a collaborative effort to investigate the molecular mechanisms underlying H<sub>2</sub>S-mediated PKM2 regulation in cancer cells.

The researchers first investigated the role of H<sub>2</sub>S in PKM2 activity through protein sulfhydration. **Figures 1(a) and 1(b)** show that treatment with NaHS, a H<sub>2</sub>S donor, induced PKM2 sulfhydration in both breast cancer MDA-MB-231 and prostate cancer PC3 cells; this modification reduced PKM2 enzyme activity, which could be reversed by dithiothreitol (DTT) treatment. Importantly, H<sub>2</sub>S caused the dissociation of fructose 1,6-bisphosphate (FBP)-induced PKM2 tetramers into monomers or dimers. This led to enhanced PKM2 nuclear translocation (**Fig. 1(c)**) and increased expression of PKM2-responsive genes, such as cyclin D1 and glutaminase-1; the expression levels of these

genes show a positive correlation with tumor growth. When  $H_2S$  was depleted using the aminooxyacetic acid inhibitor or by knocking down  $H_2S$ -producing enzymes, such as cystathionine  $\beta$ -synthase and cystathionine  $\gamma$ -lyase, both PKM2 sulfhydration and nuclear translocation decreased.

Through mass spectrometry analysis, the researchers identified two sulfhydration sites on recombinant PKM2: cysteines 49 and 326. However, only cysteine 326 was found to be endogenously sulfhydrated in MDA-MB-231 cells. To further study the effects of sulfhydration at this site, they created a mutation replacing cysteine 326 with serine (PKM2<sup>C326S</sup>). This mutation significantly reduced PKM2 sulfhydration and, notably, resulted in increased tetramer formation compared to wild-type PKM2 (**Fig. 1(d)**). Crystal structure analysis revealed that PKM2<sup>C326S</sup> adopts a unique tetrameric conformation that is different from previously known conformations (**Fig. 2(a)**). The X-ray diffraction data were collected at **TPS 07A** of the NSRRC.

The functional consequences of blocking PKM2 sulfhydration at C326 were substantial. The PKM2<sup>C326S</sup> mutation increased pyruvate kinase activity and led to significant metabolic changes in cells. Cells expressing PKM2<sup>C326S</sup> showed increased oxygen consumption rates and enhanced mitochondrial oxidative phosphorylation, while extracellular acidification rates only slightly increased. These cells also showed reduced expression of most PKM2-responsive genes, decreased levels of glycolytic intermediates, and reduced nuclear translocation of PKM2.

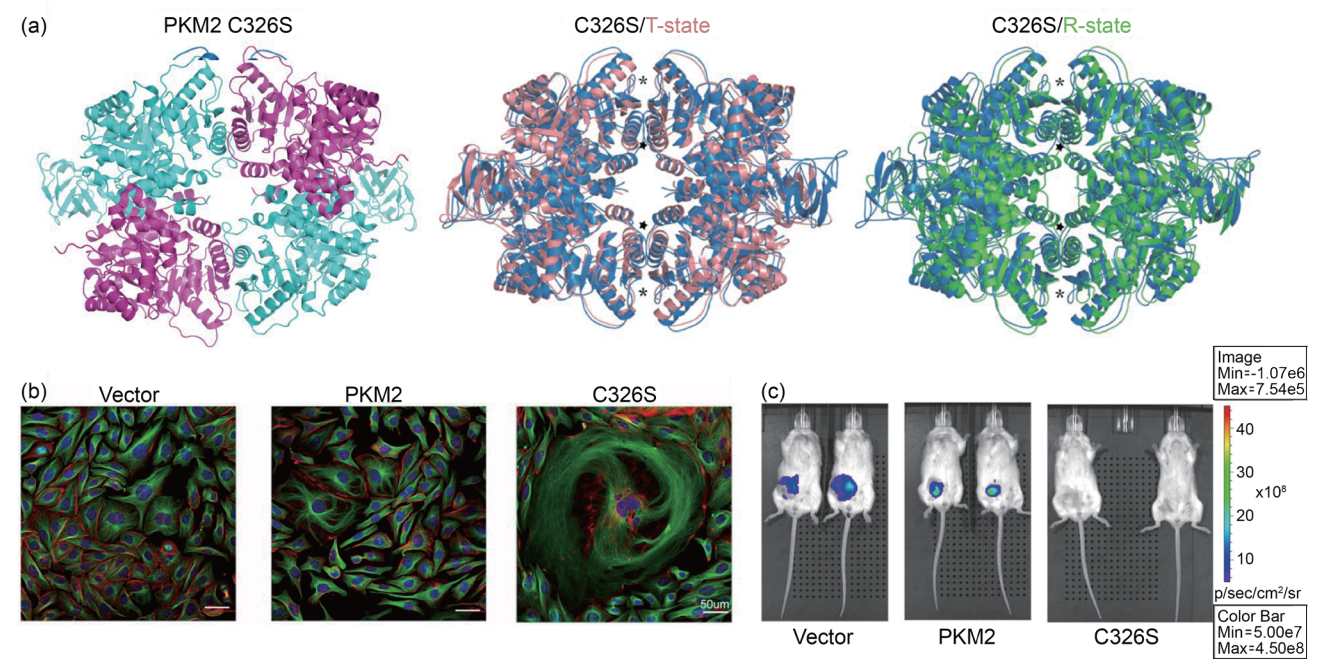


Fig. 2: (a) Structural analysis comparison of the crystal structure of PKM2 C326S mutant with both T-state (phenylalanine-bound) and R-state (FBP/serine-bound) conformations, highlighting key regions: the effector loop and α14-α15 regions, which are indicated by asterisk and star, respectively. The overlaid structures are color-coded as C326S mutant in blue, T-state in pink, and R-state in green to allow for direct comparison of conformational differences between these states. (b) Immunostaining of MDA-MB-231 cells expressing vector, PKM2, or PKM2<sup>C326S</sup>, showing actin (red), α-tubulin (green), and nuclei (DAPI, blue). Images are displayed at 50 μm scale. (c) Bioluminescence imaging of tumor growth in mouse mammary fat pads at week 7 post-implantation of MDA-MB-231 cells expressing different PKM2 variants (vector, wild-type, or C326S). [Reproduced from Ref. 2]

The researchers observed significant negative effects on cancer cell division and proliferation in cells expressing PKM2<sup>C326S</sup>. These cells showed an increased percentage of polyploidy cells and a higher frequency of giant multinucleated cells (**Fig. 2(b)**). Time-lapse microscopy revealed a 1.5-fold increase in cytokinesis failure in PKM2<sup>C326S</sup>-expressing cells. Furthermore, PKM2<sup>C326S</sup> failed to interact with the spindle checkpoint protein BUb3, and cells showed reduced proliferation rates. Similar effects were observed in cells with H<sub>2</sub>S depletion, supporting the specific role of sulfhydration in these processes.

Perhaps most significantly, in a mouse xenograft model, tumor growth was completely suppressed in the PKM2<sup>C326S</sup> group (**Fig. 2(c)**). While there were no significant differences in mouse body weight between groups, there was a dramatic reduction in tumor bioluminescence signals in the PKM2<sup>C326S</sup> group, indicating strong anti-tumor effects.

These comprehensive results demonstrate that  $H_2S$ -mediated sulfhydration of PKM2 at C326 is a crucial mechanism regulating cancer cell metabolism. Blocking this modification through the PKM2<sup>C3268</sup> mutation leads to the stabilization of PKM2 tetramers, enhanced oxidative phosphorylation, reduced nuclear translocation and transcriptional activity, impaired cell division, and

suppressed tumor growth. These findings suggest that targeting PKM2 sulfhydration could be a promising therapeutic approach for cancer treatment, particularly by rewiring glucose metabolism from aerobic glycolysis to oxidative phosphorylation. The study provides both mechanistic insights into cancer metabolism and potential therapeutic strategies for future drug development. (Reported by Chun-Hsiang Huang)

This report features the work of Hui-Chun Cheng and her collaborators published in Nat. Commun. 15, 7463 (2024).

#### TPS 07A Micro-focus Protein Crystallography

- Protein Crystallography
- Biological Macromolecules, Protein Structures, Life Science

#### References

- B. D Paul, S. H Synder, Nat. Rev. Mol. Cell Biol. 13, 499 (2012).
- R.-H. Wang, P.-R. Chen, Y.-T. Chen, Y.-C. Chen, Y.-H. Chu, C.-C. Chien, P.-C. Chien, S.-Y. Lo, Z.-L. Wang, M.-C. Tsou, S.-Y. Chen, G.-S. Chiu, W.-L. Chen, Y.-H. Wu, L. H.-C. Wang, W.-C. Wang, S.-Y. Lin, H.-J. Kung, L.-H. Wang, H.-C. Cheng, K.-T. Lin, Nat. Commun. 15, 7463 (2024).

## Structure of the Prc-Nlpl-MepS Complex: Elucidating the Regulatory Mechanism of Bacterial Cell Walls

This study reveals how the adaptor protein NIpI regulates the activity and cellular levels of the cell wall endopeptidase MepS, which facilitates peptidoglycan remodeling and maintains cell wall integrity during bacterial growth and development.

Peptidoglycan (PG) is vital for protecting bacterial cells from osmotic pressure. It consists of linear glycan strands of alternating *N*-acetylglucosamine (NAG) and *N*-acetylmuramic acid (NAM), linked to short peptide chains. The main cross-linking of the short peptide chains is the 4–3 linkage between D-Ala and meso-diaminopimelic acid (DAP), forming a net-like structure that prevents osmotic rupture. During cell growth, the net-like structure must be cleaved to incorporate new PG strands, a process facilitated by several endopeptidases, including MepS, MepM, and MepH. In *Escherichia coli* (*E. coli*), these three endopeptidases are essential for cell wall expansion and their absence leads to abnormal cell shapes and lysis.

NlpI is an outer membrane-anchored lipoprotein found in Gram-negative bacteria (*e.g.*, *E. coli*) and plays multiple roles in cell division, cell wall metabolism, virulence, and host interactions. It interacts with various hydrolases and associates with the PG synthesis machinery, influencing the stability of cell envelope components. As an adaptor protein, NlpI can bind to three endopeptidases—MepS, MepM, and PBP4—and facilitates the formation of trimeric complexes (*e.g.*, MepS-NlpI-PBP4). In addition, NlpI helps localize these enzymes, connecting PG hydrolysis to expansion. Reconstitution experiments show that NlpI organizes PG multienzyme complexes, suggesting it aids in integrating hydrolases and synthases during PG expansion.

MepS is abundant during the log phase of cell growth but declines in the stationary phase. Its protein levels within the cell are regulated by the periplasmic PDZ-protease Prc (also called tail-specific protease), in complex with the adaptor NlpI. Without NlpI, Prc cannot effectively degrade MepS, highlighting NlpI's crucial role in MepS recruitment. Mutants lacking Prc or NlpI show increased MepS levels, leading to long filaments and growth defects in low-osmolarity conditions.

In 2017, the structure of the Prc-NlpI complex (PDB ID 5WQL) was determined by X-ray crystallography, revealing a symmetric NlpI homodimer attached to two bowl-shaped Prc proteins. NlpI, an adaptor protein with four tetratricopeptide repeats (TPRs), interacts with Prc through TPR2, forming an extensive electrostatic network. The unliganded PDZ domain of Prc has a misaligned conformation, which rearranges upon ligand binding, activating its proteolytic activity (Fig. 1(a)).¹ However, two important issues regarding the regulation mechanism of PG expansion have not been resolved, namely how NlpI regulates MepS to affect their activities and how NlpI modulates the protein levels of MepS in the presence of the Prc protease. To investigate the mechanisms underlying these two important issues, Shiou-Ru Tzeng (National Taiwan University) and her collaborators U-Ser Jeng (NSRRC) and Chun-Hsiang Huang (NSRRC) employed various experimental techniques, including nuclear magnetic resonance (NMR), biological small-angle X-ray scattering (BioSAXS), protein crystallography (PX), and other biochemical analysis methods. Specifically, X-ray diffraction and scattering data were acquired using the beamlines TPS 05A, TPS 07A, and TPS 13A at the NSRRC.

To elucidate how NlpI regulates MepS, NMR experiments were performed (**Fig. 1(b)**) and demonstrated that the mature full-length MepS (mMepS) can utilize its intrinsically disordered N-terminal region to interact with the adaptor protein NlpI. The crystal structure of the NlpI-mMepS complex reveals a heterohexameric assembly, where a homodimer of NlpI binds to four MepS molecules (**Fig. 1(c)**). This structural arrangement facilitates the colocalization and cooperative function of multiple MepS molecules, enhancing their avidity for PG binding and hydrolysis. Notably, upon binding to NlpI, the disordered N-terminal region of MepS undergoes a transition to an ordered state (**Fig. 1(d)**), promoting the dimerization of MepS. This structural insight provides a mechanistic understanding of how NlpI regulates the activity of MepS through modulating its oligomerization state and cooperative interactions with the PG substrate.

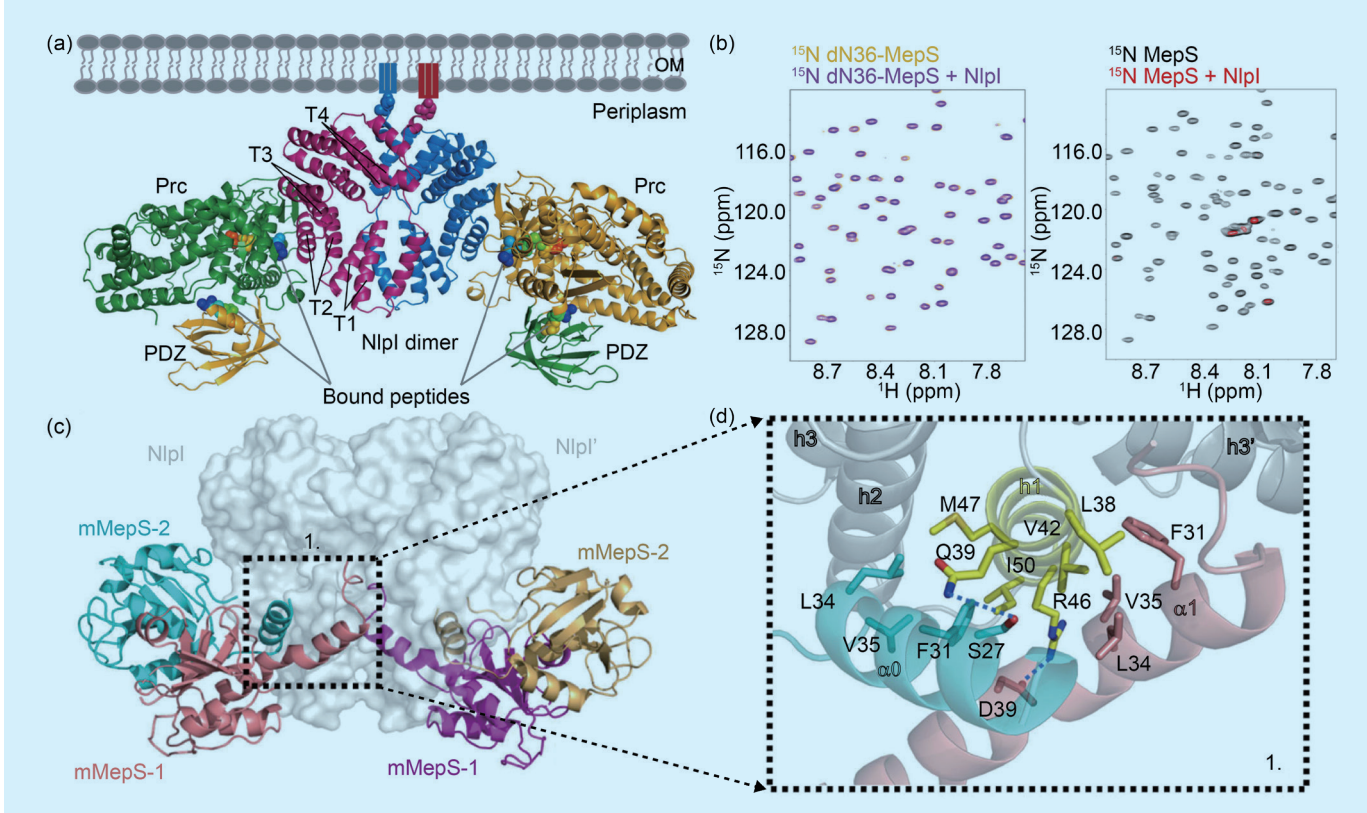


Fig. 1: (a) Overall structure of the NlpI-Prc complex shows a dimeric NlpI bound to two Prc proteins, represented in different colors. The PDZ domain of Prc and the four tetratricopeptide repeats (TPR1-4) of NlpI are labeled. The outer membrane (OM) and lipid anchors are depicted, with the first residues linked to the lipobox cysteine shown as spheres. Four co-crystallized substrate peptides are shown as rainbow-colored spheres. (b) NMR experiments were performed to study the interaction between NlpI and the mMepS proteins. <sup>1</sup>H-<sup>15</sup>N TROSY-HSQC spectra were acquired for the truncated mutant dN36-MepS, which is devoid of the N-terminal 36 residues, and mMepS in the absence and presence of unlabeled NlpI dimer. (c) Overall structure of the NlpI-mMepS complex reveals a dimeric NlpI (grey surface) bound to four mMepS proteins (illustrated in different colors). (d) The interactions between NlpI and mMepS involve specific hydrophobic contacts. [Reproduced from Ref. 1 and Ref. 2]

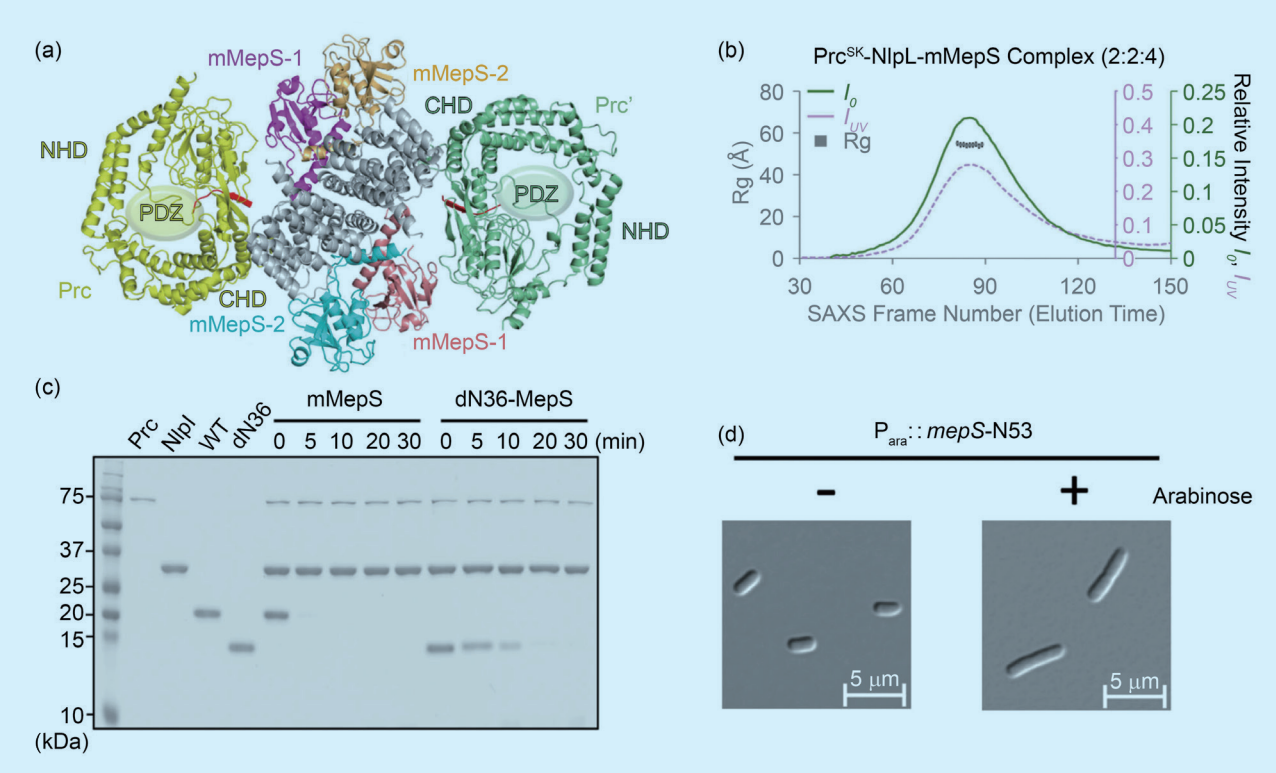


Fig. 2: (a) Overall structure of the Prc–NlpI-mMepS complex is shown, with NlpI in gray, Prc in yellow and pale green, and mMepS1 and mMepS2 in other colors. (b) A size-exclusion chromatogram of the Prc–NlpI-mMepS complex is presented, displaying the radius of gyration (*Rg*), zero-angle scattering intensity (*I*<sub>0</sub>), and absorbance at 280 nm (*I*<sub>UV</sub>). (c) *In vitro* degradation assays were conducted to examine the proteolytic activity of the Prc–NlpI system on mMepS and dN36-MepS. (d) The impact of overexpressing MepS-N53 on bacterial cell morphology was visualized using differential interference-contrast (DIC) microscopy. [Reproduced from Ref.1]

To understand how NlpI modulates the protein levels of MepS in the presence of the Prc protease, structural analysis was performed and revealed that the tail-specific protease Prc forms a 2:2:4 hetero-octameric complex with the adaptor protein NlpI and the endopeptidase mMepS (Fig. 2(a)). Size exclusion chromatography coupled with smallangle X-ray scattering (SEC-SAXS) experiments confirmed this 2:2:4 stoichiometry, ruling out the possibility that the observed stoichiometry was an artifact of crystal packing (Fig. 2(b)). Furthermore, the experimental data showed that the dN36-MepS significantly reduced its interaction with NlpI and decreased the degradation efficiency of mMepS by the Prc-NlpI system (Fig. 2(c)). This further confirms the important role of the N-terminal region in the recognition of mMepS by NlpI and the subsequent targeting of mMepS for Prc-mediated degradation. At the cellular level, overexpression of the N-terminal 53 residues of mMepS (MepS-N53) led to a significant change in bacterial morphology, resulting in the formation of long filamentous cells (Fig. 2(d)).

This study provides crucial structural insights into how the lipoprotein NlpI recruits and colocalizes the endopeptidase MepS, facilitating enhanced PG hydrolysis during bacterial cell growth. The binding of NlpI induces a disorder-to-order transition in the N-terminal region of MepS, promoting its dimerization and increasing enzymatic activity. Additionally, NlpI plays a pivotal role in targeting MepS for degradation by the protease Prc during

the stationary phase, thus regulating the cellular levels of MepS and maintaining cell wall integrity. These findings advance our understanding of the molecular mechanisms underlying bacterial cell wall remodeling and highlight the functional versatility of NlpI in coordinating PG synthesis and degradation. (Reported by Chun-Hsiang Huang, NSRRC)

This report features the work of Shiou-Ru Tzeng and her collaborators published in Nat. Commun. **15**, 5461 (2024).

### TPS 05A Protein Microcrystallography TPS 07A Micro-focus Protein Crystallography

- Protein Crystallography
- Biological Macromolecules, Protein Structures, Life Science

#### TPS 13A Biological Small-angle X-ray Scattering

- BioSAXS
- Structural Transitions of Macromolecules in Solution

#### References

- M.-Y. Su, N. Som, C.-Y. Wu, S.-C. Su, Y.-T. Kuo, L.-C. Ke, M.-R. Ho, S.-R. Tzeng, C.-H. Teng, D. Mengin-Lecreulx, M. Reddy, C.-I Chang, Nat. Commun. 8, 1516 (2017).
- S. Wang, C.-H. Huang, T.-S. Lin, Y.-Q. Yeh, Y.-S. Fan, S.-W. Wang, H.-C. Tseng, S.-J. Huang, Y.-Y. Chang, U-S. Jeng, C.-I Chang, S.-R. Tzeng, Nat. Commun. 15, 5461 (2024).